Journal of The Electrochemical Society, **164** (4) H164-H169 (2017)
0013-4651/2017/164(4)/H164/6/$37.00 © The Electrochemical Society

Electrochemical Reduction of Carbon Dioxide on Zinc-Modified Copper Electrodes

Gopalram Keerthiga[a,b,c] and Raghuram Chetty[a,b,*,z]

[a]*Chemical Engineering Department, Indian Institute of Technology Madras, Chennai, India*
[b]*National Center for Catalysis Research, IIT Madras, Chennai, India*
[c]*Chemical Engineering Department, BMS College of Engineering, Bangalore, India*

Electrochemical reduction of carbon dioxide (CO_2) was performed on zinc-deposited copper (Cu/Zn) electrodes, and the faradaic efficiency of this system toward methane, ethane, and hydrogen was evaluated. Hierarchically structured Zn was electrodeposited on a Cu substrate under constant voltage in a varying bath concentration of Zn to yield low- and high-concentration deposits, represented as Cu/Zn-A and Cu/Zn-B, respectively. The prepared materials were characterized by X-ray diffraction, scanning electron microscopy, and X-ray photoelectron spectroscopy. The reduction of CO_2 was performed with the Cu/Zn electrodes in an H-type cell, and the results obtained were compared with those from bare Cu and Zn electrodes, revealing that a high deposit of Zn on Cu (Cu/Zn-B) shows greater conversion efficiency than does a low Zn deposit (Cu/Zn-A) and the maximum faradaic efficiency of methane follows the order Cu/Zn-B (52%) > Cu (23%) > Zn (7%). Moreover, the efficiency of hydrogen formation is suppressed on Cu/Zn-B (8%) compared to bare Cu (68%) in the potential range studied. The results suggest that depositing Zn on Cu favors a protonation reaction, which results in higher C_1 product formation on a Cu/Zn-B electrode.
 [DOI: 10.1149/2.0421704jes]

Manuscript submitted September 1, 2016; revised manuscript received January 9, 2017. Published January 27, 2017.

Carbon dioxide (CO_2) emissions contribute significantly to challenging environmental problems.[1] CO_2 is an abundant, nontoxic, stable, nonflammable, and easily obtained carbon source. Substantial research is being carried out on its potential in synthesizing specialty chemicals and raw materials,[2,3] and several authors have reviewed ways to use CO_2 efficiently.[4–6]

Electrochemical method is an attractive route for the conversion of CO_2 to useful products at ambient conditions, and the identification of a low-cost electrocatalyst with high selectivity is a central research focus. Copper (Cu), a medium hydrogen overvoltage metal, is one of the cost-effective electrocatalysts studied widely in various forms, such as unmodified bare Cu,[7,8] Cu nanofoams,[9] Cu nanowires,[10] and Cu mesocrystals,[11] while modifications such as oxidation,[12,13] ultrasonic treating,[14] plasma activation,[15] depositing Cu on Cu,[3,16,17] and the formation of bimetallic Sn-Cu,[18] Ni-Cu,[19] Pd-Cu,[20] and Au-Cu[21] aim to activate and reduce CO_2. These electrocatalysts assist in multielectron transfer to yield CO ($2e^-$), methanol ($6e^-$), methane ($8e^-$), and ethane ($14e^-$) based on the number of electrons transferred during the reduction,[22] which can be generally represented by Equation 1:

$$CO_2 + H_2O + \text{energy} \rightarrow CH_xO_y + zO_2 \qquad [1]$$

Many authors have studied the theoretical and experimental evidence influencing the effects of surface morphology on the selectivity of Cu[7,9,23–26] with the broad aim of achieving a stable and selective electrode. Thermodynamically, formation of methane and ethylene should occur at a lower cathodic potential than hydrogen on copper electrodes; however, kinetically, this is not the case.[2] Hence, apart from Cu-based electrocatalysts, other medium hydrogen overvoltage metals like Zn, Au, and Ag have also been explored for the reduction of CO_2.[24,27–29]

In general, product selectivity depends on parameters like the nature of the electrode, electrolyte, pH, and potential applied.[30] The supporting electrolyte influences the solubility and modes of adsorption of intermediates during CO_2 reduction. Aqueous[3,31] and nonaqueous electrolytes[32] have been examined with Cu-based cathode, and halide electrolytes have been commonly reported to show promising results toward CO_2 reduction via suppression of the adsorption of protons and mitigation of the overpotential of the reduction.[30,31]

Zn, an amphoteric metal, is available in abundance and is cheaper than Cu. It is one among several metals that have been screened for CO_2 reduction in aqueous (bicarbonate) and nonaqueous electrolytes, with lower hydrogen evolution having been reported (<40%) in several studies.[24,33] In the recent times, hierarchically structured electrodes have attracted much attention for CO_2 conversion due to their high catalytic surface area and unique properties compared to their polycrystalline counterparts, for example Rosen et al.[34] reported nanostructured dendritic Zn catalyst capable of reducing CO_2 to CO in aqueous bicarbonate electrolyte over an order of magnitude higher than the bulk Zn counterpart, with 3 times higher faradaic efficiency for CO.

Normally, hydrogen evolution occurs more slowly on Zn electrode than on Cu electrode,[34] hence, one approach to enhance the electrocatalytic activity of Cu electrode toward CO_2 reduction is to form bimetallic Cu-Zn catalyst. Katah et al.[35] studied the catalytic activity of electrodeposited Cu-Zn alloys on gold substrate for CO_2 reduction in aqueous bicarbonate solution at 2°C and reported one order of magnitude higher efficiency for CO on Cu-Zn alloy than that for pure Cu or pure Zn. Andrews et al.[36] reported the electrochemical reduction of CO_2 in aqueous bicarbonate electrolyte using Cu nanoclusters on single crystal (1010) ZnO electrode, hydrogen evolution occurred with a faradaic efficiency of 45% on Cu/ZnO compared to 54% on Cu electrode. While the faradaic efficiencies of other products were similar for both the electrodes, the selectivity improved by an order of magnitude for the Cu/ZnO electrode.

The choice of the alloying metal and electrodeposition conditions influence the structure and properties of the resultant Cu-based electrode, which in turn affect their electrocatalytic activity and product selectivity toward CO_2 reduction.[1,2,35] Although few studies have been devoted to develop bimetallic Cu-Zn catalyst toward CO_2 reduction, no explicit study on the deposition of hierarchical Zn structures on Cu substrate, toward the electroactivity of CO_2 reduction have been reported. In this study, hierarchically structured Zn electrocatalyst on Cu electrode was synthesized using a simple electrodeposition method. The bath concentration of Zn was varied during electrodeposition to yield Cu/Zn-A (a low-concentration deposit of Zn on Cu) and Cu/Zn-B (a high-concentration deposit of Zn on Cu). The electrochemical reduction of CO_2 on a Zn-deposited Cu substrate was carried out, and the performance of the electrocatalyst was compared in terms of its faradaic efficiency and partial current density with pure Zn and Cu electrodes.

Experimental

Preparation and characterization of Zn on Cu.—A commercially available Zn sheet (Alfa Aesar) was polished with emery paper (220 grade) to remove surface oxide and was then degreased with acetone and washed with distilled water. A constant voltage was employed to deposit the Zn at −0.3 V vs. platinum (Pt) for 15 minutes in a three-

*Electrochemical Society Member.
[z]E-mail: raghuc@iitm.ac.in

electrode setup containing pretreated Cu as the working electrode, Zn as the counter electrode, and platinum (Pt) as the reference electrode.[37] The Cu electrode was polished with emery paper (220 grade) and treated in 1 M H_2SO_4 and 1 M H_3PO_4 for 10 to15 minutes[17] to remove surface impurities. Then the electrode was degreased with acetone, washed with distilled water, and dried in a nitrogen atmosphere.

An aqueous solution of sodium zincate was used as an electrolytic bath. Two different electrolytic bath concentrations were chosen for Zn deposition, and these were henceforth designated Cu/Zn-A for 0.6 M sodium zincate and Cu/Zn-B for 6 M sodium zincate. Deposition was repeated for uniformity and was characterized via scanning electron microscopy (SEM), X-ray diffraction (XRD), and X-ray photoelectron spectroscopy (XPS). The XRD patterns of the bare and deposited electrodes were obtained with an X-ray diffractometer (PANalytical X'Pert PRO) using Cu K_α radiation at 45 kV and 20 mA. The scan rate was $0.04^\circ min^{-1}$ in the range $2\theta = 10^\circ$–90°. Images of the deposited electrodes were obtained with a Hitachi S4800 FESEM equipped with an energy-dispersive analytical system (Horiba EDX). XPS measurements were carried out in an ultrahigh vacuum setup equipped with a Gamma data- Scienta SES 2002 analyzer. A monochromatic Al K_α (a 1486.6 eV anode operating at 14 kV and 55 mA) X-ray source was used as incident radiation. Binding energies were calibrated using the C1s peak of graphite at 284.5 eV as a reference.

Electroreduction of CO_2.—All electrochemical experiments were carried out in an H-type cell separated by a glass frit. Ag/AgCl (3.5 M saturated KCl) and Pt foil were used as reference and counter electrodes, respectively. In the results, potential is expressed with respect to a normal hydrogen electrode (NHE) unless otherwise specified, where V vs. NHE = V vs. Ag/AgCl + 0.197. All experiments were carried out at room temperature (23 ± 1°C). A solution of 0.5 M KCl (Merck) prepared in Milli-Q water (ρ18.2 MΩ · cm) was used as an electrolyte. Electrochemical measurements were performed using an EC Epsilon potentiostat in the electrolyte saturated with CO_2.

The pH of the solution was measured using a pH/ion meter (Eutech Instruments). Cyclic voltammetry measurements were carried out in an N_2 saturated solution (blank) and compared with those carried out in a CO_2 saturated solution. Potential was scanned between 0 V and−1.2 V vs. NHE and was reported at a sweep rate of 10 mV s^{-1}. The faradaic efficiency of the products obtained was calculated from the ratio of the mass of the substance actually liberated via electrolysis to the mass of the substance obtained as per Faraday's law as represented by Equations 2, 3, and 4[38], and partial current density was calculated by the product of faradaic efficiency and current density,

$$Q_i = n_i F C_i V \quad [2]$$

$$Q_t = j_i A t_i \quad [3]$$

$$\text{Faradaic efficiency} = \frac{Q_i}{Q_t} \times 100\% \quad [4]$$

where Q_i is the theoretical charge based on the product yield, Q_t is the actual charge measured, F is the faradaic constant (96,485 C mol^{-1}), n_i is the number of electrons involved in the reaction, C_i is the observed concentration (mol m^{-3}), V is the volume of the reaction cell (ml), j_i is the current density (A m^{-2}), A is the electrode area (m^2), and t_i is the time interval (s).

Product analysis.—Gaseous products obtained during the electroreduction were analyzed at regular intervals manually via gas chromatography using a PerkinElmer Clarus 800 equipped with a PoraPLOT Q column and a molecular sieve column. FID and TCD detectors were used to analyze hydrocarbons and hydrogen, respectively, with N_2 as a carrier gas. The liquid phase products were analyzed via gas chromatography, high-performance liquid chromatography using a Chromatopak C-18 column with a UV detector, and titrimetric analysis. No significant liquid products were observed. Hence, only gaseous products were accounted for, as any liquid phase products were considered below the detectable limit. In this study, the products are expressed in millimoles/micromoles per unit of geometric area ($1cm^2$) of the electrode and by faradaic efficiency.

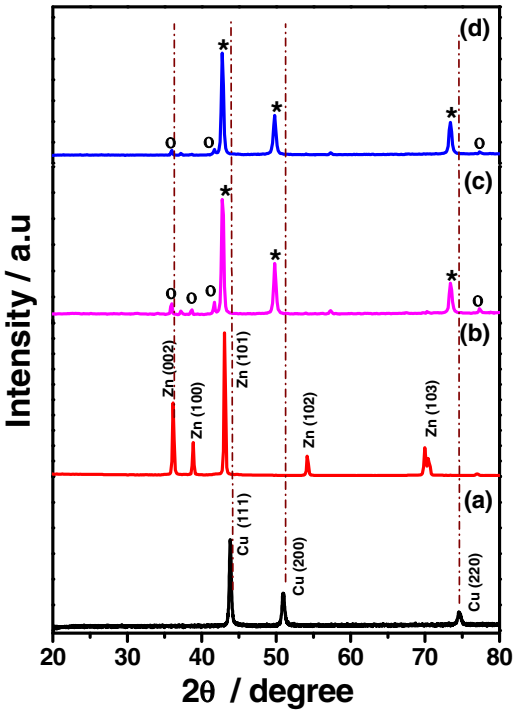

Figure 1. X-ray diffraction patterns: (a) bare Cu, (b) bare Zn, (c) Zn deposited at 0.6 M bath concentration for 15 min (Cu/Zn-A), (d) Zn deposited at 6 M bath concentration for 15 min (Cu/Zn-B) where * and **o** corresponds to Cu-Zn solid solution and $CuZn_2$ cubic structure, respectively.

Results and Discussion

Catalyst characterization.—The thickness of the electrodeposited Zn was calculated using Equation 5,[17]

$$\frac{M_w}{nFAD} \int (I \times t) \quad [5]$$

where M_w is the molecular weight of the sample, n is the number of electrons involved in the deposition, F is Faraday's constant (96,485 C mol^{-1}), A is the surface area of the deposited electrode (1 cm^2), and D is the density of the Zn metal (7.1 g cm^{-3}).

The weight of the deposit was calculated by measuring the difference in the weight of the Cu sheet before and after the deposition. The thickness and weight of the Cu/Zn-A electrode were found to be 11 μm and 0.01 mg, respectively, whereas the thickness and weight of the Cu/Zn-B electrode were found to be 28 μm and 0.1 mg, respectively.

The samples were examined by X-ray diffraction, and Fig. 1 shows the XRD patterns of Cu, Zn, and electrodeposited Cu/Zn. Figs. 1a and 1b correspond to bare Cu and bare Zn in accordance with their reported diffraction peaks (Cu: JCPDS 04-0836, Zn: JCPDS 00-004-0831). The electrodeposited Cu/Zn-A and Cu/Zn-B catalysts showed similar XRD patterns, with major reflections around 42.7°, 49.8°, and 73.4°, which can be ascribed to fcc Cu-Zn solid solution,[35] while the minor reflections around 36.2°, 38.6° and 77.3° can be attributed to cubic $CuZn_2$.[35]

Scanning electron microscopic images of electrodeposited Zn on Cu and bare Zn are shown in Fig. 2, and a representative EDX plot for Cu/Zn-A is shown in Fig. 3. Fig. 2a corresponds to bare Zn, and Fig. 2b corresponds to Zn deposited from a 0.6 M sodium zincate solution (Cu/Zn-A), showing uniform hexagonal Zn structures with growing whisker-like crystals oriented perpendicular to the substrate.

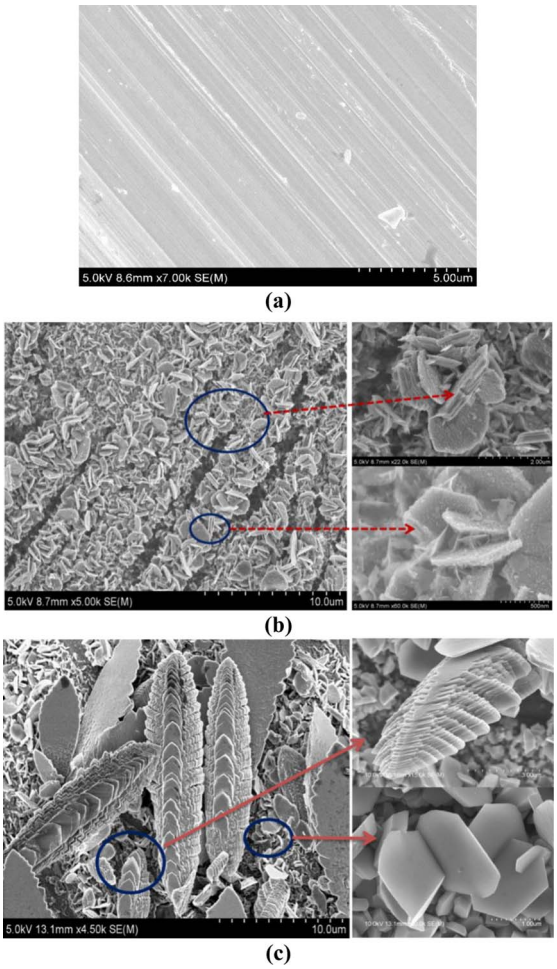

Figure 2. Scanning electron micrographs: (a) bare Zn, (b) Zn deposited from 0.6 M sodium zincate bath solution (Cu/Zn-A), and (c) Zn deposited from 6 M sodium zincate bath solution (Cu/Zn-B). Deposition time: 15 min. Deposition potential: −0.3 V.

Then, as the concentration is increased to 6 M, an intercalated hexagonal cubic Zn structure is observed to have been deposited on the Cu electrode (Cu/Zn-B) (Fig. 2c). Moreover, the fully grown cubes rearrange as dendritic structures. Thus, hierarchical structures of dendrites grow on the surface because of the effects of the bath concentration, which appear porous, offers a higher surface area and alters the crystallographic orientation and crystallinity of the metal deposit.[39] The

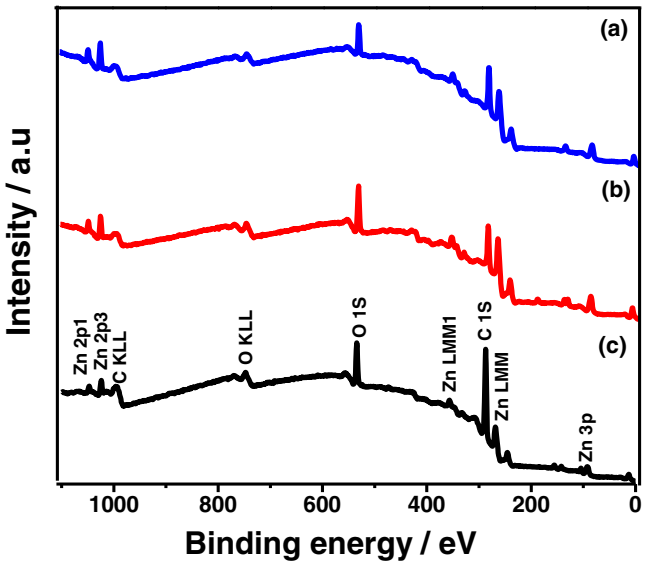

Figure 4. XPS survey spectra: (a) Cu/Zn-B, (b) Cu/Zn-A and (c) bare Zn electrode.

deposited electrodes, when characterized by EDX, revealed the presence of Cu, Zn, and O on the surface (Fig. 3).

The surface chemical species of Zn electrodeposited on the Cu electrode were analyzed via XPS. The overall survey spectra and regional O1s spectra of the samples are shown in Fig. 4 and Fig. 5. The elemental composition calculated from the regional spectra showed a high carbon content resulting from carbonaceous species found on the substrate probably after exposure to air,[40] and the absence of characteristic Cu peaks in the survey spectra was possibly due to a thicker Zn deposit on the Cu electrode.

The O1s region was deconvoluted into three peaks around 530.1, 531.2, and 532.5 eV as shown in Fig. 5. The peak at 530.1 ± 0.5 eV can be attributed to chemisorbed oxygen, whereas the peaks at 531.2± 0.5 eV and 532.5 ± 0.5 eV can be attributed to adsorbed hydroxyl (OH) species and surface oxygen on the samples, respectively.[41] The area of the oxide peak at 530.1 ± 0.5 eV (Fig. 5) varies in the ratio of 2:1 for Cu/Zn-B and Cu/Zn-A.

Cyclic voltammetry of Zn and Zn-modified electrodes.—The cyclic voltammogram (CV) of the Zn electrode in the 0.5 M KCl supporting electrolyte is shown in Fig. 6, where the dotted line corresponds to the CV of the N_2 saturated solution (pH 6.1) and the solid line corresponds to the CO_2 saturated solution (pH 4.9). The shift in

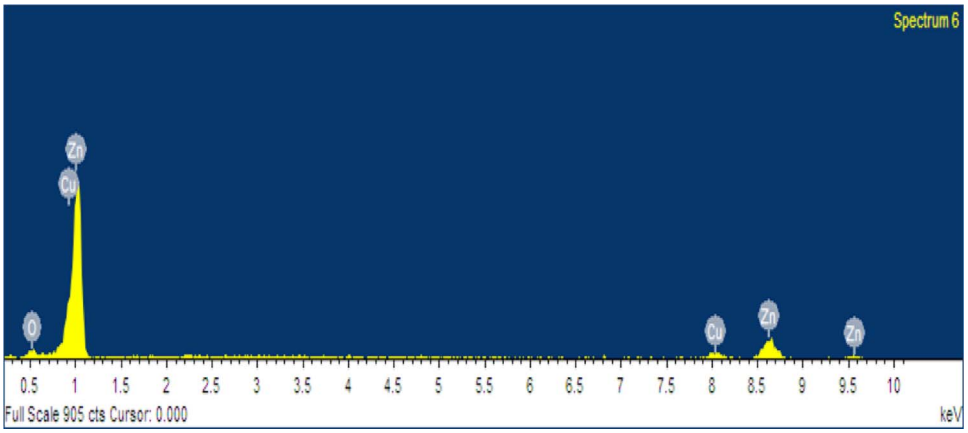

Figure 3. A representative EDX spectra of Cu/Zn-A.

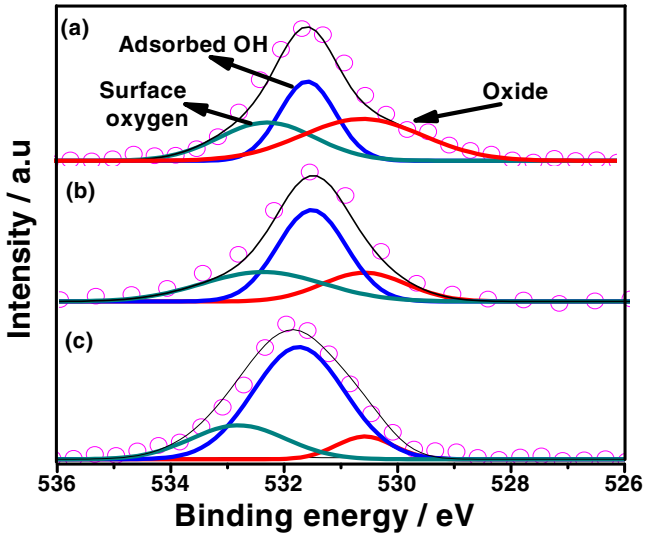

Figure 5. Individual O1s spectra: (a) Cu/Zn-B, (b) Cu/Zn-A, and (c) bare Zn electrode.

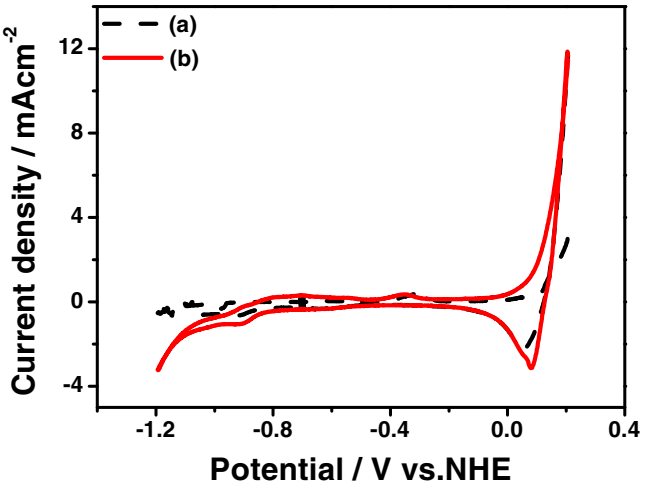

Figure 7. Cyclic voltammogram of Cu/Zn-B in 0.5 M KCl at scan rate of 10 mV s^{-1} (a) N_2 saturated solution (dotted line) and (b) CO_2 saturated solution (solid line).

the onset of the reduction of Zn in the N_2 saturated (−0.64 V) and CO_2 saturated solutions (−0.74 V) could be due to a corresponding change in system pH from 6.1 to 4.9 during CO_2 purging.[28] An increased current density of 10 mA cm^{-2} was observed at −0.97 V for the CO_2 saturated solution compared to the N_2 saturated solution, which indicates a catalytic interaction between CO_2 and halide ions as well as an accelerated electron transfer to CO_2 and its subsequent reduction.[30]

Fig. 7 shows a representative plot of the voltammetric behavior of the deposited Cu/Zn-B electrode in a N_2 saturated solution (dotted line) and a CO_2 saturated solution (solid line). The onset of the CO_2 saturated solution occurred at −0.84 V compared to −0.9 V for the N_2 saturated solution. An increased current density of 2.5 mA cm^{-2} at −1.2 V for the CO_2 saturated solution in comparison to the N_2 saturated solution is analogous to the behavior of the Zn electrode discussed above in Fig. 6.

Reaction studies.—Electrolysis was carried out with a KCl electrolyte in an H-type cell by varying the electrode potential, and product formation was monitored over four hours. To evaluate the products formed during CO_2 reduction, a time-dependent study of Zn/Cu electrodes was carried out when no detectable products other than methane, ethane, and hydrogen were observed when analyzed by gas chromatography–mass spectrometry. Fig. 8a represents the products formed on the Cu/Zn-A electrode, and Fig. 8b represents the products formed on the Cu/Zn-B electrode at a potential of −1.4 V vs. NHE. An average methane formation of 59.4 μmol cm^{-2}, ethane formation of 18.7 μmol cm^{-2}, and hydrogen formation of 22.7 mmol cm^{-2} was

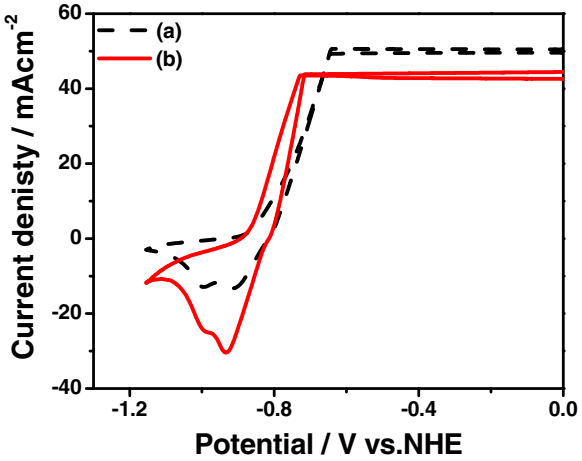

Figure 6. Cyclic voltammogram of Zn electrode in 0.5 M KCl at scan rate of 10 mV s^{-1} (a) N_2 saturated solution (dotted line) and (b) CO_2 saturated solution (solid line).

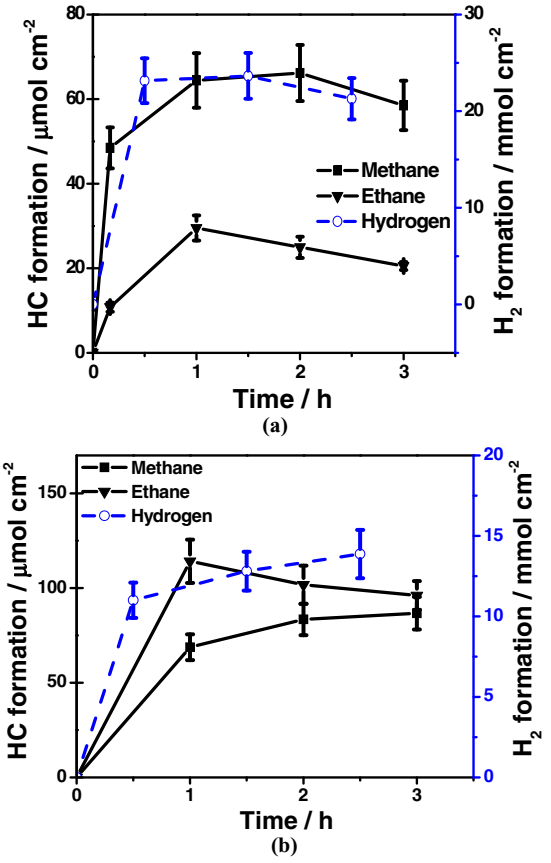

Figure 8. Effect of electrolysis time on the products formed during CO_2 reduction in KCl electrolyte on electrodeposited Cu electrodes at −1.4 V in (a) Cu/Zn-A and (b) Cu/Zn-B.

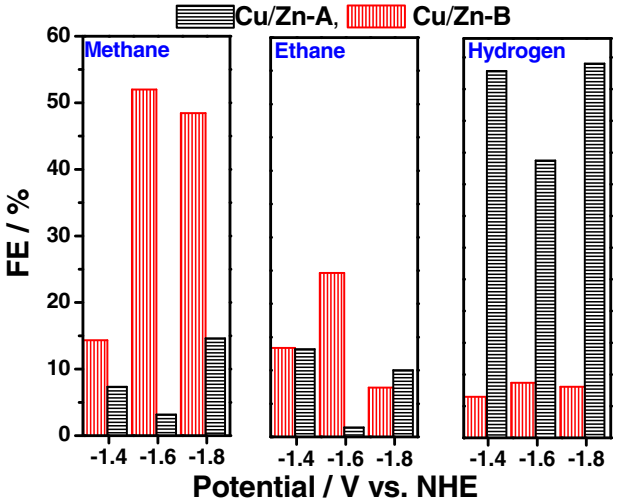

Figure 9. Comparison of faradaic efficiency vs. potential for the products formed during CO_2 reduction on Cu/Zn-A and Cu/Zn-B electrodes in 0.5 M KCl.

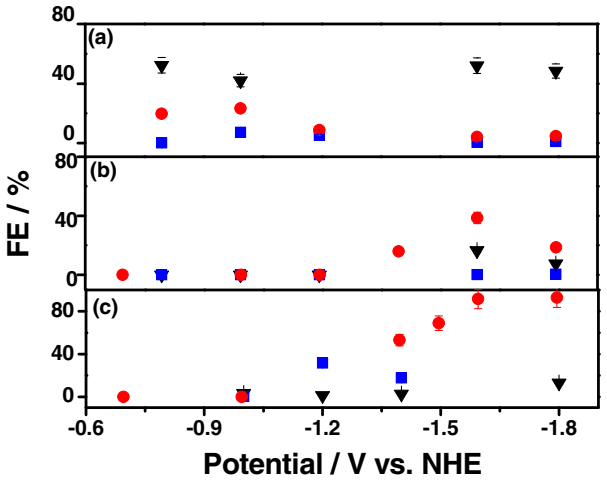

Figure 10. Plot of faradaic efficiency (FE) vs. potential for (a) methane, (b) ethane, and (c) hydrogen on Cu/Zn-B (▼), Cu (●) and Zn (■) electrode in 0.5 M KCl electrolyte.

obtained on the Cu/Zn-A electrodes, while an average methane formation of 79.6 μmol cm^{-2}, ethane formation of 97.3 μmol cm^{-2}, and hydrogen formation of 13.2 mmol cm^{-2} was obtained from the Cu/Zn-B electrodes. This demonstrates that Cu/Zn-B yields more methane (79.6 μmol cm^{-2}) and ethane (97.3 μmol cm^{-2}) when compared at a particular potential. Hence, the variation of products over a range of potentials was studied to determine the effect of potential and the overall activity of the electrode.

The potential of the working electrode was therefore varied from −0.7 V to −1.8 V vs. NHE, and its faradaic efficiency was evaluated. Fig. 9 shows a comparative analysis of the product formed on the Cu/Zn-B and Cu/Zn-A electrodes as a function of potential. A maximum methane formation of 52%, ethane formation of 24%, and H_2 formation of 8.7% was observed at a potential of −1.6 V on the Cu/Zn-B electrode, whereas the Cu/Zn-A electrode showed lower hydrocarbon formation and higher hydrogen evolution. The behavior with respect to hydrocarbon formation can be attributed to the Cu electrode,[7] whereas the behavior with respect to hydrogen formation can be compared to that of the Zn electrode.[27,42] Hence, in further studies, we limited our discussion only to hierarchical dendritic structure of Cu/Zn-B, and the results were compared with those of bare Cu and Zn electrodes.

Fig. 10 shows a comparison plot of the faradaic efficiency (FE) of the products formed versus the potential on Cu/Zn-B, Cu, and Zn electrodes. The faradaic efficiency of methane (Fig. 10a) on the Cu/Zn-B electrode was found to be higher (average efficiency of 50%) than on the Cu and Zn electrodes. For example, at a potential of −1.6 V, the faradaic efficiency of Cu/Zn-B was 52% compared to that of Cu (4%) and Zn (1%). Hence, we have found that dendritic Zn deposited on the Cu electrode enhanced the selectivity of the C_1 product. Ethane formation was negligible on the Cu and Cu/Zn-B electrodes until −1.2 V. With a further increase in potential, ethane formation increased, giving maximum faradaic efficiencies of 38% and 16% at −1.6 V for Cu and Cu/Zn-B, respectively, as shown in Fig. 10b. On the other hand, the Zn electrode did not favor ethane formation throughout the potential range studied. Similarly, as depicted in Fig. 10c, the faradaic efficiency for hydrogen was higher on the Cu electrode than on the Zn and Cu/Zn-B electrodes. At −1.4 V, Cu electrode evolved 53% hydrogen than compared to 3% on Cu/Zn-B and 18% on Zn. The total faradaic efficiency less than 100% signifies the possibility of unidentified products in the reaction.

Copper is probably the best-known metal catalyst for electrochemically converting CO_2 into hydrocarbons. However, the competing reactions limit the yield of single product, and the catalyst stability is attributed to surface blocking by intermediates of the reduction process.[7] Reduction of CO_2 occurs effectively in aqueous solution also on metal electrodes such Zn, which has rather high overpotential for hydrogen evolution.[33] Nevertheless, in the literature, information about Zn electrodes for CO_2 reduction is not as general as in the case of Cu.

Surface modification by electrodeposition can result in porous Cu-Zn electrodes[43] and produce active sites different from those of a polycrystalline metal.[44] Moreover, the synergism between Cu and Zn sites in Cu/Zn catalysts for methanol synthesis is well known,[45] where addition of Zn minimizes the surface energy and prevents the oxidation of metallic Cu.[46] In the present work, the deposition of hierarchically structured Zn which is porous in nature on the Cu electrode could allow CO_2 to diffuse through to the Cu/Zn interface for the reduction, and sustain high catalytic activity because of the large electrode area of the hierarchical structure slowing down the surface poisoning. Cu catalyzes the reduction of CO_2, and the presence of porous hierarchical Zn lower the hydrogen evolution. In such an arrangement, product selectivity could be enhanced with the synergism and active sites of Cu-Zn interface, which favors C1 formation at lower potential rather than forming C-C bond which needs higher potential. Nevertheless, the combined effect of deposition of Zn on Cu electrode for CO_2 reduction needs further mechanistic insights.

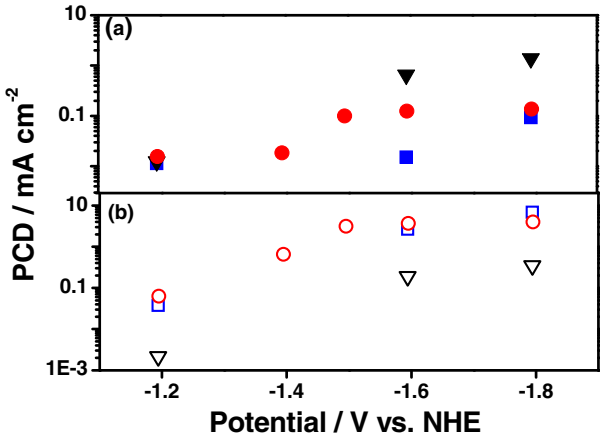

Figure 11. Partial current density vs. potential for (a) methane and (b) hydrogen formed during CO_2 reduction on Cu/Zn-B (▽,▼), bare Cu (●, ○) and bare Zn (■,□) electrodes in 0.5 M KCl electrolyte.

Fig. 11 shows the partial current density plots for methane and hydrogen obtained during CO_2 reduction on the Cu, Zn, and Cu/Zn-B electrodes. Partial current density helps in assessing the reaction rate[47] and is given by the product of individual current density and faradaic efficiency. No significant change in the current density was observed until −1.2 V, whereas at potentials above −1.2 V Cu/Zn-B exhibited a higher current density for methane with lower hydrogen evolution. At a potential of −1.6 V, a higher current density for the Cu/Zn-B electrode (0.70 mA cm^{-2}) was observed, which ensured higher methane formation compared to the Cu (0.14 mA cm^{-2}) and Zn (0.01 mA cm^{-2}) electrodes. Similarly, lower hydrogen evolution (0.19 mA cm^{-2}) on the Cu/Zn-B electrode ensured less formation of byproducts during the reduction. Thus, dendritic Zn deposited on Cu electrode results in varied current density, which results in selective hydrocarbon formation.

Cu is known for its hydrogenating property, while Zn is known for lower hydrogen evolution.[29] Hence, the deposition of Zn on Cu was attempted, and the resulting Cu/Zn-B exhibited Cu characteristics through favoring the addition of protons to form methane (faradaic efficiency 52%) and Zn characteristics through lower hydrogen evolution (faradaic efficiency 8%).

Conclusions

The electrochemical reduction of CO_2 was studied on a Zn-deposited Cu electrode, and its faradaic efficiency was compared to that of bare Cu and Zn electrodes. Cu catalyzes the reduction of CO_2, and the presence of porous and hierarchically structured Zn lower the hydrogen evolution. In such an arrangement, the product selectivity could be enhanced with the synergism and active sites of Cu-Zn interface favoring C1 formation. Time-dependent and potential-dependent studies of Cu/Zn-B showed higher methane formation and lower hydrogen evolution. Moreover, the faradaic efficiency of methane was enhanced on the Cu/Zn-B (52%) electrode compared to the bare Cu (23%) electrode. The efficiency of hydrogen on the Cu/Zn-B electrode was significantly reduced compared to that on the Cu electrode. These results suggest that methane is the desired product on Cu/Zn-B, as deposition of Zn on Cu lowers hydrogen evolution.

Acknowledgment

We thank Prof. B. Viswanathan, National Centre for Catalysis Research (NCCR), Indian Institute of Technology (IIT) Madras for his valuable suggestions and fruitful discussions. Thanks are also due to Indian Oil Corporation Limited (IOCL), R&D Centre, Faridabad for the fellowship to GK. We acknowledge the support of Department of Science and Technology (DST) for funding National Centre for Catalysis Research (NCCR) and DST-FIST for providing the instrumentation facility to the Department of Chemical Engineering, IIT Madras.

References

1. H. Kim, I Choi, S.H. Ahn, S.J. Hwang, S.J. Yoo, J. Han, J. Kim, H. Park, J.H. Jang, and S. Kim, *International Journal of Hydrogen Energy*, **39**, 16506 (2014).
2. M. Gattrell, N. Gupta, and A. Co, *Journal of Electroanalytical Chemistry*, **594**, 1 (2006).
3. M. R. Goncalves, A. Gomes, J. Condeço, R. Fernandes, T. Pardal, C. A. C. Sequeira, and J. B. Branco, *Journal of Energy Conversion and Management*, **51**, 30 (2010).
4. C. Costentin, M. Robert, and J. M. Saveant, *Chemical Society Reviews*, **42**, 2423 (2013).
5. J. L. Rern, X. Mingshi, A. S. Mahasin, M. L. Jong, F. Adrian, W. Xin, and H. L. Kok, *Catalysis Today*, **233**, 169 (2014).
6. K. Ruud, S. Jing, J. P. S. Klaas, C. V. Federico, and T. M. K. Marc, *Journal of Physical Chemistry Letters*,**6**, 4073 (2015).
7. K. P. Kuhl, E. R. Cave, D. N. Abram, and T. F. Jaramillo, *Energy and Environmental Science*, **5**, 7050 (2012).
8. W. Li, *American Chemical Society Symposium Series*, **1056**, 55, (2010).
9. S. Sen, D. Liu, G. Tayhas, and R. Palmore, *ACS Catalysis*, **4**, 3091 (2014).
10. R R. David, J. L.Kenneth, and W. Chao, *Nano Letters*,**15**, 6829 (2015).
11. C. S. Chen, A. D. Handoko, J. H. Wan, L. Ma, D. Rena, and B. S. Yeo, *Catalysis Science and Technology*, **5**, 161 (2015).
12. C. W. Li and M. W. Kanan, *Journal of American Chemical Society*, **134**, 7231 (2012).
13. G. Keerthiga, B. Viswanathan, C. A. Pullikottil, and R. Chetty, *Bonfring International Journal of Industrial Engineering and Management Science*, **2**, 41 (2012).
14. K. Ohta, K. Suda, S. Kaneco, and T. Mizuno, *Journal of the Electrochemical Society*, **147**, 233 (2000).
15. M. Hemma, S. V. Ana, S. B. Cecile, Z. Ioannis, S. Ilya, C. Yong-Wook, K. Kim, A. S Eric, C. Y. Judith, S. Peter, and R. C. Beatriz, *Nature Communications*, **7**, 12123 (2016).
16. M. R. Goncalves, A. Gomes, J. Condeo, T. R. C. Fernandes, T. Pardal, C. A. C. Sequeira, and J. B. Branco, *Electrochimica Acta*, **102**, 388(2013).
17. G. Keerthiga, B. Viswanathan, and R. Chetty, *Catalysis Today*, **245**, 68 (2015).
18. H. Li and C. Oloman, *Journal of Applied Electrochemistry*, **35**, 955 (2005).
19. S. Kaneco, Y. Sakaguchi, H. Katsumata, T. Suzuki, and K. Ohta, *Bulletin of the Catalysis Society of India*, **6**, 74 (2007).
20. Y. Zhen, G. Dunfeng, Y. Siyu, Z. Bo, C. Fan, L. Lili, T. Pei, Z. Peng, W. Guoxiong, M. Ding, and B. Xinhe, *Nano Energy*, **27**, 35 (2016).
21. C. Jihui, J. K. Myung, H. A. Sang, C. Insoo, H. J. Jong, S. H. Yu, J. K. Jae, and K. K. Soo, *Chemical Engineering Journal*, **299**, 37 (2016).
22. A. Michele, D. Angela, and A. Antonella, *Journal of CO_2 Utilization*, **3**, 65 (2013).
23. W. Tang, A. A. Peterson, A. S. Varela, Z. P. Jovanov, L. Bech, W. J Durand, S. Dahl, and J. K. Norskov, Chorkendorff, *Physical Chemistry Chemical Physics*, **14**, 76 (2012).
24. K. Hara, A. Kudo, and T. Sakata, *Journal of Electroanalytical Chemistry*, **391**, 141 (1995).
25. X. Nie, M. R. Esopi, M. J. Janik, and A. Asthagiri, *Angewandte Chemie International Edition*, **52**, 2459 (2013).
26. A. A. Sneha, T. M. Ian, and M. J. Janikz, *Journal of the Electrochemical Society*, **163**, F477 (2016).
27. S. Kaneco, K. Iiba, K. Ohta, T. Mizuno, and A. Saji, *Journal of Electroanalytical Chemistry*,**441**, 215 (1998).
28. S. Kaneco, K. Iiba, K. Ohta, T. Mizuno, and A. Saji, *Electrochimica Acta*, **44**, 573 (1998).
29. V. S. K. Yadav and M. K. Purkait, *Solar Energy*, **124**, 177 (2016).
30. H. Yano, T. Tanaka, M. Nakayama, and K. Ogura, *Journal of Electroanalytical Chemistry*, **565**, 287 (2004).
31. K. Ogura, *Journal of CO_2 Utilization*, **1**, 43 (2013).
32. A. M. Rizzuto, R. L Pennington, and K. D. Sienerth, *Electrochimica Acta*, **56**, 5003 (2011).
33. M. Karamad, V. Tripkovic, and J. Rossmeisl, *ACS Catalysis*, **4**, 2268 (2014).
34. J. Rosen, G. S. Hutchings, Q. Lu, R.V. Forest, A. Moore, and F. Jiao, *ACS Catalysis*, **5**, 4586 (2015).
35. A. Katah, H. Uchida, M. Shibata, and M. Watanabe, *Journal of the Electrochemical Society*, **141**(8) 2054 (1994).
36. E. Andrews, F. Wang M.Ren, Z. Zhang, P. Sprunger, R. Kurtz, and J. Flake, *Journal of the Electrochemical Society*, **160** (11), H841 (2013).
37. R. Winand, Electrodeposition of Zinc and Zinc Alloys. In *Modern Electroplating*; M. Schlesinger and M. Paunovic, Eds., 5th ed.; John Wiley & Sons Inc. New Jersey (2010).
38. B. R. Eggins, C. Ennis, R. Mcconnell, and M. Spence, *Journal of Applied Electrochemistry*, **27**, 706 (1997).
39. A. Gomes and M. I. D. Silva Pereira, *Electrochimica Acta* , **51**, 1342 (2006).
40. S. Colin, E. Beche, R. Berjoan, H. Jolibois, and A. Chambaudet, *Corrosion Science*, **41**, 1051 (1999).
41. X. Deng, A. Verdaguer, T. Herranz, C. Weis, H. Bluhm, and M. Salmeron, *Langmuir*, **24**, 9474 (2008).
42. K. Hara, A. Tsuneto, A. Kudo, and T. Sakata, *Journal of Electroanalytical Chemistry*, **434**, 239 (1997).
43. L. Mattarozzi, S. Cattarin, N. Comisso, R. Gerbasi, P. Guerriero, M. Musiani, L. V. Gómez, and E. Verlato, *Journal of Electrochemical Society*, **162**, D236 (2015).
44. A. M. Appel, J. E. Bercaw, A. B. Bocarsly, H. Dobbek, D. L. DuBois, M. Dupuis, J. G. Ferry, E. Fujita, R. Hille, P. J. A. Kenis, C. A. Kerfeld, R. H. Morris, C. H. F. Peden, A. R. Portis, S.W. Ragsdale, T. B. Rauchfuss, J. N. H. Reek, L.C. Seefeldt, R.K. Thauer, and G.L. Waldrop, *Chemical Reviews*, **113**, 6621 (2013).
45. H.Y. Chen, S.P. Lau, L. Chen, J. Lin, C.H.A. Huan, K.L. Tan, and J.S. Pan, *Applied Surface Science*, **152**, **193**, (1999).
46. D. Grandjean, V. Pelipenko, E. D. Batyrev, J. C. Van den Heuvel, A.A. Khassin, T. M. Yurieva, and B. M. Weckhuysen, *Journal of Physical Chemistry C*, **115**, 20175 (2011).
47. Z. He, J. Shen, Z. Ni, J. Tang, S. Song, J. Chen, and L. Zhao, *Catalysis Communications*, **72**, 38 (2015).